

Polyoxopalladates Encapsulating Yttrium and Lanthanide Ions, [X^{III}Pd^{II}₁₂(AsPh)₈O₃₂]⁵⁻ (X = Y, Pr, Nd, Sm, Eu, Gd, Tb, Dy, Ho, Er, Tm, Yb, Lu)

Maria Barsukova,^[a] Natalya V. Izarova,^[a, e] Rosa Ngo Biboum,^[b] Bineta Keita,^[b] Louis Nadjo,^[b] Vasanth Ramachandran,^[c] Naresh S. Dalal,^[c] Nadya S. Antonova,^[d] Jorge J. Carbó,^[d] Josep M. Poble, ^[d] and Ulrich Kortz*^[a]

Dedicated to Professor Walter G. Klemperer on the occasion of his 63rd birthday

Abstract: A series of novel yttrium- and lanthanide-containing heteropolyoxopalladates have been prepared and isolated as hydrated sodium salts, Na₅[X^{III}Pd^{II}₁₂(AsPh)₈O₃₂]^{y-}·yH₂O (X = Y (1), Pr (2), Nd (3), Sm (4), Eu (5), Gd (6), Tb (7), Dy (8), Ho (9), Er (10), Tm (11), Yb (12), Lu (13); y = 15–27). The polyanions [X^{III}Pd^{II}₁₂(AsPh)₈O₃₂]⁵⁻ consist of a cuboid framework of twelve Pd^{II} ions with eight phenylarsonate heterogroups located at the vertices and a central guest ion X. The compounds 1–13 have been prepared in a simple one-pot self-assembly reaction of Pd(CH₃COO)₂, phenylarsonic acid and the respective salt of the element X in 0.5 M aqueous sodium acetate solution (pH 6.9), and characterized in

the solid state by single-crystal X-ray diffraction, elemental and thermogravimetric (TGA) analyses, and IR spectroscopy. It was demonstrated that small, medium, and also large lanthanide ions can be incorporated in the center of the novel heteropolyoxopalladate [X^{III}Pd^{II}₁₂(AsPh)₈O₃₂]⁵⁻. The Ln–O bond lengths follow the expected trend decreasing from left to right in the lanthanide series. This indicates that the {Pd^{II}₁₂O₃₂} shell can adjust to the coordination requirements of the encapsu-

lated guest cation. Compounds 3 and 5 were selected for electrochemical studies. Their cyclic voltammetry in a lithium acetate buffer at pH 5.9 showed a Pd⁰ deposition process on the glassy carbon electrode surface. Coulometry indicated that all Pd^{II} centers were reduced to Pd⁰. The film was stable and could be taken out of the deposition medium and characterized in pure pH 5.9 buffer. Magnetic susceptibility and EPR measurements were carried out on 5 and 6. The former was confirmed to be diamagnetic and the latter strongly paramagnetic with a S = 7/2 ground state. DFT calculations for some of the polyoxometalates have been also performed.

Keywords: density functional calculations · electrochemistry · lanthanides · magnetism · palladium · polyoxometalates


[a] M. Barsukova, Dr. N. V. Izarova, Prof. U. Kortz
School of Engineering and Science
Jacobs University
P.O. Box 750 561, 28725 Bremen (Germany)
Fax: (+49) 421-200-3229
E-mail: u.kortz@jacobs-university.de

[b] R. N. Biboum, Dr. B. Keita, Prof. L. Nadjo
Laboratoire de Chimie Physique
UMR 8000, CNRS
Equipe d'Electrochimie et Photoelectrochimie
Université Paris-Sud, Bâtiment 350, 91405 Orsay Cedex (France)

[c] V. Ramachandran, Prof. N. S. Dalal
Department of Chemistry and Biochemistry
Florida State University
32306 Tallahassee, FL (USA)

[d] N. S. Antonova, Dr. J. J. Carbó, Prof. J. M. Poble
Department de Química Física i Inorgànica
Universitat Rovira i Virgili, 43007 Tarragona (Spain)

[e] Dr. N. V. Izarova
Permanent address: Nikolaev Institute of Inorganic Chemistry
SB RAS, Prospekt Lavrentyeva 3, 630090 Novosibirsk (Russia)

 Supporting information for this article is available on the WWW under <http://dx.doi.org/10.1002/chem.201000631>.

Introduction

Polyoxometalates (POMs) comprise a large class of polynuclear metal–oxygen clusters usually formed by early-transition elements in high-oxidation states, such as Mo⁶⁺, W⁶⁺, or V⁵⁺, and mixtures of these elements.^[1] As a result of their structural diversity, redox properties, solubility in various media, high charges and ionic weights, POMs have a wide range of applications, such as catalysis, medicine, electronics, multifunctional materials, and analytical chemistry.^[2]

The area of noble metal based POMs was pioneered by Wickleder et al. with the preparation of [Pt^{III}₁₂O₈(SO₄)₁₂]⁴⁻ by reaction of Pt(NO₃)₂ with H₂SO₄ at 350 °C.^[3] Some years later our group discovered a simple open-beaker procedure for the synthesis of late-transition-metal oxo complexes in aqueous media. We have prepared the first example of a polyoxopalladate(II), [Pd^{II}₁₃As^V₈O₃₄(OH)₆]⁸⁻,^[4a,b] and very recently also the first polyoxoaurate [Au^{III}₄As^V₄O₂₀]⁸⁻.^[4c] The pentagonal star-shaped polyoxopalladates [Pd₁₅P₁₀O₅₀]²⁰⁻ and [Pd₁₅(μ₃-SeO₃)₁₀(μ₃-O)₁₀Na]⁹⁻ and the two 13-palladate derivatives [Pd₁₃(PhAs)₈O₃₂]⁶⁻ and [Pd₁₃Se₈O₃₂]⁶⁻ (**Pd**₁₃) have also been reported.^[5] In the latter two species, the eight AsO₄³⁻ capping groups of [Pd^{II}₁₃As^V₈O₃₄(OH)₆]⁸⁻ have been replaced by phenylarsonate(V) and a lone pair containing selenite(IV), respectively. Interestingly, the nature of the external heterogroup influences the coordination geometry of the central Pd^{II} ion leading to unusual coordination numbers, such as six in [Pd₁₃Se₈O₃₂]⁶⁻ and even eight in **Pd**₁₃.^[5b]

This prompted us to further study the structural and electronic flexibility and stability of the heteropoly-12-palladate shell. We set out to investigate systematically which main group, transition metal, or rare-earth elements could possibly be placed in the center of the {Pd₁₂L₈} structure. The incorporation of lanthanide ions into POM frameworks has already led to compounds with interesting luminescence, magnetic, and Lewis acid catalytic properties.^[6] Moreover, using lanthanide ions has allowed the construction of solid 1D, 2D, or 3D POM assemblies as well as very large discrete polyanions.^[7]

Here, we report on the synthesis, structure, electrochemistry, magnetic properties, and DFT calculations of the heteropolyoxopalladate family Na₅[X^{III}Pd^{II}₁₂(AsPh)₈O₃₂]⁵⁻·yH₂O with encapsulated Y (**1**) and lanthanide ions (X = Pr (**2**), Nd (**3**), Sm (**4**), Eu (**5**), Gd (**6**), Tb (**7**), Dy (**8**), Ho (**9**), Er (**10**), Tm (**11**), Yb (**12**), Lu (**13**); y = 15–27).

Results and Discussion

Synthesis and structure: Dark red-brown crystals of **1–13** have been prepared in a simple one-pot self-assembly reaction of Pd(CH₃COO)₂, phenylarsonic acid, and the respective lanthanide(III) or yttrium (III) salt in 0.5 M aqueous sodium acetate solution (pH 6.9) in yields ranging from 9% (for **2**) to 43% (for **1**). These compounds are stable towards

air and light in the solid state and can be successfully recrystallized several times from water.

The compounds **1–13** are all isomorphous and crystallize in the tetragonal crystal system in the space group *I4/m* and they. The structure of the {XPd₁₂(AsPh)₈O₃₂} core is very similar to that in the previously reported **Pd**₁₃ and can be described in terms of Platonic and Archimedean solids.^[4b] The main difference is that the central Pd^{II} ion in the latter has been replaced by a Ln^{III} or Y^{III} ion (see Figure 1).

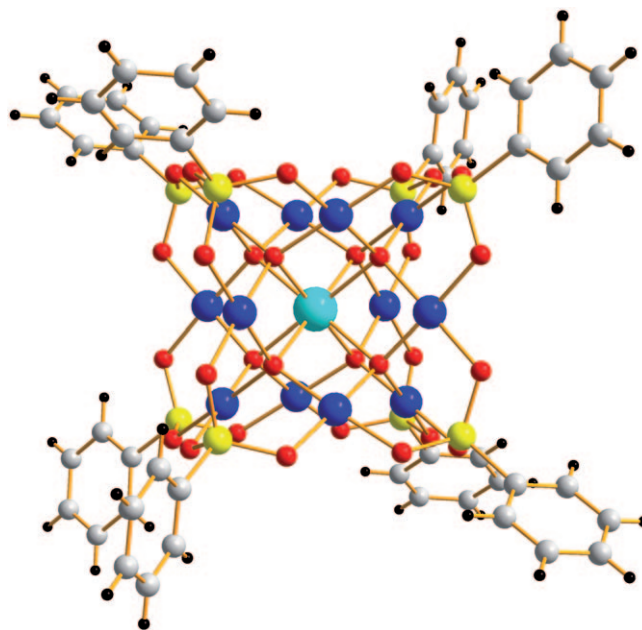


Figure 1. Ball-and-stick representation of [X^{III}Pd^{II}₁₂(AsPh)₈O₃₂]⁵⁻. Color code: X turquoise, Pd blue, As yellow, O red, C gray, and H black.

This central yttrium or lanthanide ion in **1–13** is coordinated by eight oxygen atoms situated at the vertices of a cube. The twelve palladium(II) ions surrounding the central {XO₈} fragment form a cuboctahedron. Each oxygen atom of the “inner” {XO₈} cube (μ₄-O) is coordinated by the lanthanide ion and by three palladiums, situated on a trigonal face of the cuboctahedron. Each of the twelve Pd^{II} ions exhibits the expected square-planar coordination by two μ₄-O and two “outer” oxygen atoms (μ₂-O). The 24 “outer” oxygen atoms form a truncated-cube shaped shell, which is capped by eight positively charged AsPh⁴⁺ groups. The eight As atoms possess tetrahedral coordination geometry and form in fact an external, cube-shaped shell. Selected bond lengths for the polyanions in **1–13** are shown in Table 1.

Thus, small, medium, and large lanthanide ions can be incorporated in the center of the heteropolyoxopalladate [X^{III}Pd^{II}₁₂(AsPh)₈O₃₂]⁵⁻. The X–O bond lengths in these polyanions decrease from **2** to **13**, following the expected trend of the lanthanide series (see Table 1). Moreover the Pd···Pd distances in the {Pd^{II}₁₂O₃₂} noble metalate host shell increase with increasing size of the encapsulated heterome-

Table 1. Selected bond lengths [\AA] for the polyanions in **1–13**.

	X-(μ_4 -O)	Pd-(μ_4 -O) (mean)	Pd-(μ -O) (mean)	As-(μ -O) (mean)	As-C
1	2.346(6)	1.994(6)	2.034(7)	1.689(7)	1.897(6)
2	2.431(4)	1.995(4)	2.022(5)	1.693(5)	1.883(3)
3	2.420(4)	1.996(4)	2.027(5)	1.693(5)	1.885(4)
4	2.386(9)	1.990(8)	2.016(10)	1.694(10)	1.899(13)
5	2.382(5)	1.991(5)	2.023(6)	1.694(6)	1.886(4)
6	2.379(8)	1.989(7)	2.022(8)	1.681(9)	1.880(6)
7	2.350(7)	2.000(7)	2.031(9)	1.695(9)	1.882(7)
8	2.349(8)	1.991(8)	2.024(10)	1.698(10)	1.885(16)
9	2.335(7)	1.992(7)	2.025(8)	1.700(8)	1.887(6)
10	2.332(11)	1.991(11)	2.028(12)	1.693(13)	1.89(2)
11	2.320(9)	1.994(9)	2.025(10)	1.697(11)	1.891(8)
12	2.329(7)	1.990(7)	2.029(8)	1.696(9)	1.882(6)
13	2.303(11)	1.994(10)	2.023(12)	1.703(12)	1.877(9)

tal guest and vice versa. This feature of the encapsulating $\{\text{Pd}^{\text{II}}_{12}\text{O}_{32}\}$ polyoxopalladate shell is exciting and suggests a certain “structural elasticity”, meaning that the host matrix adjusts to the size and coordination requirements of the incorporated guest cation.

In the solid state the polyanions in **1–13** form a hexagonal-packing framework with channels along the *a* axis (see Figure 2). The channels are occupied by crystal water mole-

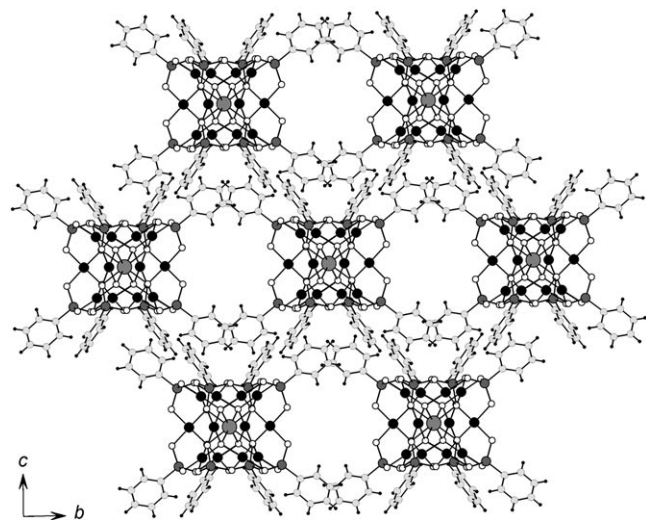


Figure 2. The hexagonal packing arrangement of the polyanions in **1–13** along the *a* axis. Sodium cations and crystal waters have been omitted for clarity. Shading code of atoms: X large gray balls, Pd black balls, As gray balls, O white balls with black border, C white balls with gray border, H small black balls.

cules and sodium counter cations. Neighboring polyanions interact through weak CH/ π hydrogen bonds,^[8] which are directed along diagonals between the *b* and *c*, and the $-b$ and $-c$ axes. There are no π - π stacking interactions between the phenyl groups, possibly because of steric hindrance or repulsion between the hydrophilic polyoxopalladate core and the hydrophobic aromatic groups.

IR spectra: The polyoxopalladate salts **1–13** and the parent $\text{Na}_6[\text{Pd}_{13}(\text{PhAs})_8\text{O}_{32}]\cdot 24\text{H}_2\text{O}$ (**Na-Pd₁₃**) have similar FT-IR spectra showing only slight shifts in some band positions.^[5b] As an example, for **1** the strong bands at $\tilde{\nu}=438$, 543, and 611 cm^{-1} correspond to the vibrational modes of the Pd-O groups, which could be superimposed with bands associated with the X-O vibrations, as we will discuss in the theoretical analysis section (vide infra). The strong band at $\tilde{\nu}=800\text{ cm}^{-1}$ is attributed to the vibrations of the $\{\text{AsO}_3\}$ fragments. The stretching and bending vibrations of the C-H and C-C bonds of the phenyl rings appear in the regions between $\tilde{\nu}=1480$ and 1094 cm^{-1} and $\tilde{\nu}=744$ – 694 cm^{-1} , respectively. The broad band at $\tilde{\nu}=1629\text{ cm}^{-1}$ belongs to asymmetric vibrations of the crystal waters.

Thermogravimetric analysis (TGA): The thermal stability of **1–13** was investigated on crystalline samples by thermogravimetric analysis under a nitrogen atmosphere. The thermogravimetric processes of **1–13** are very similar and reveal several weight-loss steps. For example, for **1** the first step occurs between 25 and 224°C and corresponds to the loss of 26 water molecules per formula unit. The number of water molecules determined by TGA is slightly lower than that obtained by crystallography (32 molecules). This fact can be easily explained by partial loss of crystal waters during sample drying. Single crystals for XRD measurements were taken directly from the mother liquid, put in oil and frozen under nitrogen flow on the diffractometer, whereas the samples for TGA were air-dried for at least one day. The combustion of eight phenyl groups per formula unit proceeds in the temperature range of 224 – 415°C . The additional smooth weight loss before 550°C is assigned to the removal of oxygen associated with the decomposition of As_2O_5 into As_2O_3 and O_2 . Several consecutive weight-loss steps covering the temperature range of 550 – 807°C are attributed to arsenic volatility, most likely in the form of As_4O_6 .^[5b,9]

Electrochemistry: The trivalent state is known to be characteristic for all lanthanides and for yttrium. The divalent state, both in solution and/or in solid compounds, was established for some of these elements, but is usually unstable. Finally, the tetravalent state (except Ce^{IV}) is rare.^[10] Then, taking standard electrode potentials into account,^[10,11] it appears that any direct interference of the redox behaviors of the yttrium or lanthanides ions in the electrochemistry of **1–13** might be, a priori, anticipated to imply their reduction from the trivalent to the divalent state^[10] or from the trivalent to the metallic state.^[11] However, these processes are unfavorable in aqueous media, because they necessitate lower reduction potentials than that of the hydrogen evolution process.^[10,11] For example, the two least unfavorable standard potentials are: -0.582 V versus SCE for $\text{Eu}^{\text{III}}/\text{Eu}^{\text{II}}$ and -1.422 V versus SCE for $\text{Yb}^{\text{III}}/\text{Yb}^{\text{II}}$.^[10] Reductions to the metallic states need even lower electrode potential values. Specific standard potentials values are: -2.614 V versus SCE^[12] for $\text{Y}^{3+}\rightleftharpoons\text{Y}$ and only slightly varying, but fairly negative standard electrode potentials (from -2.762 V

vs. SCE for La^{III}/La to -2.492 V vs. SCE for Lu^{III}/Lu) are known in the lanthanide series.^[11] In addition, experimental potentials may shift to even more negative values, to an extent depending on the stabilization effects of the supporting electrolyte anion. As a consequence, if considering the standard potential of the Pd⁰/Pd^{II} redox couple ($E^0 = +0.709$ V vs. SCE^[12]), the electrochemistry of the present complexes should be dominated by the redox behaviors of the Pd^{II} centers. Also, deposition of Pd⁰ is anticipated, a circumstance that will favor hydrogen evolution and thus further limit the possibilities to reach very low potentials. The Nd derivative **3** was selected as a representative example for electrochemical studies. A complementary reason dictating this choice is that **3** exhibited one of the best solubilities in the tested buffers amongst all compounds of the series. The particular case of compound **5** was also considered because the Pd^{II} and the Eu^{III} centers are both electroactive in aqueous solution. Figure 3 shows the evolution of the cyclic vol-

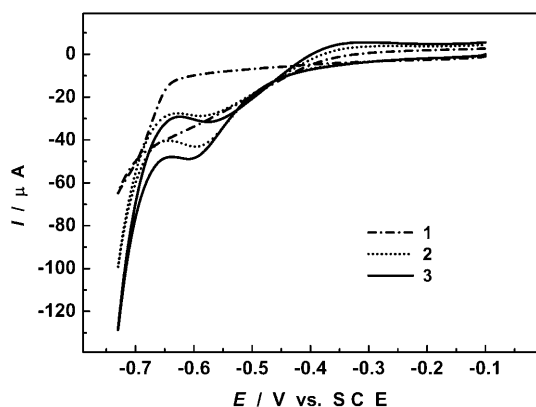


Figure 3. Representative cyclic voltammograms observed upon cycling repeatedly a glassy carbon electrode in a 4×10^{-5} M **3** in 1 M (CH₃COOLi/H⁺) pH 5.9 buffer solution in the potential domain from -0.100 to -0.730 V versus SCE. Working electrode: glassy carbon; reference electrode: SCE; scan rate: 2 mV s^{-1} . For further details, see text.

tammograms (CVs) observed for 4×10^{-5} M **3** in 1 M (CH₃COOLi/H⁺) pH 5.9 buffer solution in the potential domain from -0.100 V to -0.730 V versus SCE.

During the very first scan starting at -0.100 V in the negative potential direction, a broad ill-defined peak is observed around -0.650 V. This wave, attributed to the reduction of Pd^{II} centers, is followed by a pattern featuring hydrogen sorption–desorption and hydrogen-evolution processes.^[4a,5b,13,14] Upon potential reversal, this wave is chemically irreversible, but the pattern is completed by a trace crossing loop indicating that the current continues to increase during this positive going scan. Such an observation in the cyclic voltammetry of **3** must be associated with the formation and growth of a new phase following a nucleation event. Analogous behavior is commonly obtained during film deposition on electrodes. In subsequent runs, the wave shape sharpens with a gradual shift of the peak potential in the positive direction. The crossover loop still persisted. These scans cause

the formation of a film on the electrode surface. As expected, the film thickness and, correlatively, the associated current intensities, increase with the number of deposition cycles.

The voltammograms run with **5** at the same conditions used for **3** also show essentially the reduction of Pd^{II} centers followed by sorption–desorption and finally evolution of hydrogen. These processes impede the observation of Eu^{III} reduction in complex **5**. In support of this conclusion, we have checked that EuCl₃, dissolved in the (CH₃COOLi/H⁺) pH 5.9 buffer, is reduced by about 0.300 V negative to the Pd^{II} reduction peak potential observed with **5**. As a consequence, the reduction wave of the Eu³⁺ center in **5** is, at best, mixed with hydrogen processes.

For both **3** and **5**, the electrodes could be taken out of the deposition solution, thoroughly rinsed with Millipore water, and studied in the pure pH 5.9 electrolyte. Figure 4 shows a

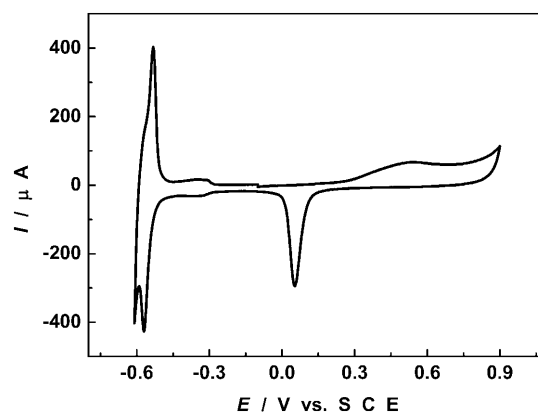


Figure 4. Characterization of the film taken out of the deposition solution containing **3**, thoroughly rinsed with Millipore water and then studied in a pure pH 5.9 (1 M CH₃COOLi/H⁺) medium.

typical example of a CV observed with the electrode prepared by using **3**. It confirms that an adherent electroactive film is deposited on the electrode surface, as described previously in the cases of several other Pd^{II}-containing POMs.^[4a,5,13] The same films could also be deposited by potentiostatic electrolysis. Controlled potential electrolyses performed with the potential of a glassy carbon plate set at -0.600 V versus SCE for **3** (or -0.500 V vs. SCE for **5**), showed that all Pd^{II} centers were reduced with the consumption of 2.0 ± 0.1 electrons per palladium ion.

Altogether, these observations support the one-step reduction of the Pd^{II} centers in **3** and **5** to Pd⁰, including a nucleation process. Analysis of Figure 4 also supports this conclusion. In short, Figure 4 exhibits essentially the same characteristics as those observed for a deposit of Pd⁰ formed from Pd^{II} on a glassy carbon electrode surface.

Specifically, the CV in Figure 4 can be divided in two potential domains to be analyzed in sequence. In the domain starting from -0.100 V to $+0.900$ V in the positive potential direction and back to -0.100 V, appears the well known composite oxidation wave of the deposited Pd⁰ surface, with

a broad peak located roughly at +0.530 V, followed upon potential reversal, by the sharp characteristic reduction wave of the Pd oxides, peaking around +0.054 V. As expected, the domain between -0.100 V and -0.600 V features all the patterns associated with the different states of hydrogen sorption-desorption. The foregoing conclusions comply with results gathered from the pertinent literature.^[4a,5b,13,14] For **3** the main hydrogen sorption-desorption wave following the Pd⁰ deposition wave exhibits an anodic to cathodic peak potential difference of $\Delta E_p = 0.038$ V. This fairly good symmetry stands in contrast to the relative asymmetry of the same process at identical experimental conditions, but using PdSO₄ for the deposition of Pd⁰, for which $\Delta E_p = 0.087$ V was measured.^[4a] Tentatively, these characteristics might be assumed to establish faster kinetics of the electrochemical Pd⁰ deposition reactions from solutions of **3** or **5** (as compared to solutions of PdSO₄). Finally, Pd⁰ films deposited from the heteropolypalladates^[4a,5b,13] appear to exhibit better characteristics than those made from 'free' Pd^{II}.

A final parameter concerns the durability of the modified electrodes. They could be kept in the atmosphere of the laboratory without any deleterious effect on their electrochemical behavior when they were soaked back in solution.

The previously described **Na-Pd₁₃** and **3** differ formally only by the replacement of the central Pd^{II} ion by a Nd^{III} ion, and so it is of interest to highlight any differences in their electrochemical behavior brought about by the lanthanide. Qualitatively, the cyclic voltammograms corresponding to these polyanions show analogous waves, but the film thickness was found to increase faster during deposition from **3** than from **Na-Pd₁₃**. Other differences appear essentially in the potential locations of the waves and in their shapes. Small variations in the potential locations of the Pd oxides reduction waves cannot be used for comparison, as this reduction is known to be a very complex process depending on several parameters.^[15] Although a chemically reversible wave is observed for **Na-Pd₁₃** in the deposition medium (reduction $E_{\text{peak}} = -0.515$ V vs. SCE) just prior to the hydrogen evolution (see Figure S7 in reference [13a]), without any visual characteristic of a deposition process, the crossover loop in the case of **3** is a clear indication of electrode filming. In addition, although a gradual positive peak potential shift is observed during the deposition of **3**, the measured peak potential remains more negative than for **Na-Pd₁₃**, at least during the first several runs. The opposite behavior would have been expected considering the five negative charges of **3** compared to the six negative charges of **Na-Pd₁₃**, if proton interference were not to play any role during the reduction processes. Therefore, it should be concluded that the presence of Nd^{III} within **3** significantly modifies its deposition pathway compared to that of **Na-Pd₁₃**.

Magnetic studies: The Gd derivative **6** exhibited temperature-dependent magnetic susceptibility and field-dependent magnetization (Figures 5 and 6). The diamagnetic correction to the measured total susceptibility was made in the usual manner, as described elsewhere.^[16] The dc susceptibility

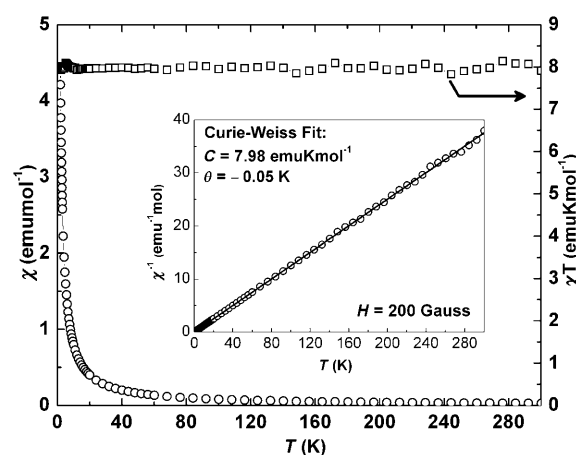


Figure 5. Temperature dependence of dc magnetic susceptibility (χ) and the product of dc susceptibility and temperature (χT), of **6** at $H = 200$ Gauss. Inset: Curie-Weiss fit to the temperature dependent inverse susceptibility, yielding the Curie constant $7.98 \text{ emu K mol}^{-1}$ corresponding to an $S = 7/2$ system, in this case, Gd^{III}.

obeyed the Curie-Weiss law. The Curie constant was found to be $7.98 \text{ emu K mol}^{-1}$, which is very close to the theoretical value ($7.87 \text{ emu K mol}^{-1}$) for an isolated Gd^{III} ion ($S = 7/2$) and the Weiss temperature was very small. The product of dc susceptibility and temperature, χT , remained constant over the entire temperature range, 1.8–300 K, with a value of 8 emu K mol^{-1} .

The field-dependent magnetization of **6** measured by varying the field from 0 to 7 T at a temperature of 1.8 K is shown in Figure 6. The saturation magnetization was $7.08 \mu_B$, very close to the theoretical value of $7 \mu_B$ corresponding to an $S = 7/2$ paramagnetic ion.^[17] The data fit very well to the Brillouin function yielding a spin of 3.5 per molecule. The Eu compound **5** did not show any magnetic behavior.

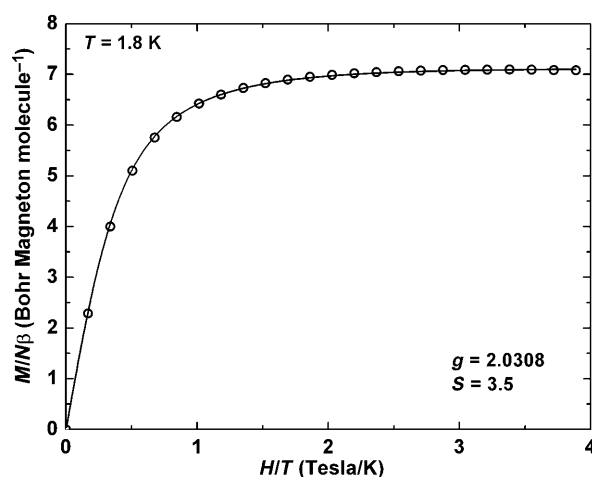


Figure 6. Field-dependent magnetization of **6**, measured at $T = 1.8$ K. The solid line represents the best fit to the Brillouin function using the parameters listed in the figure. The observed saturation magnetization, $M_S = 7.08 \mu_B$, is close to the expected $M_S = 7 \mu_B$ for an $S = 7/2$ system, Gd^{III} in this case.

The EPR spectrum of a paramagnetic molecule with spin S , can be described by the following standard spin Hamiltonian given by Equation (1),

$$H = \beta \vec{H} \cdot \vec{g} \cdot \hat{S} + D \hat{S}_z^2 + B_4^0 \hat{O}_4^0 + B_4^4 \hat{O}_4^4 \quad (1)$$

in which β is the Bohr magneton, g is the Lande g tensor, S is the total spin with components S_x , S_y , and S_z , with z being taken to be the direction along which the Zeeman field H is applied. D is the zero-field splitting parameter. O_4^0 and O_4^4 are the Stevens operators denoting fourth-order zero-field interactions and B_4^0 and B_4^4 are the corresponding zero-field splitting parameters.^[18] The room-temperature EPR spectrum of a single crystal of **6**, with its long axis oriented parallel to the magnetic field, is shown in Figure 7. The spec-

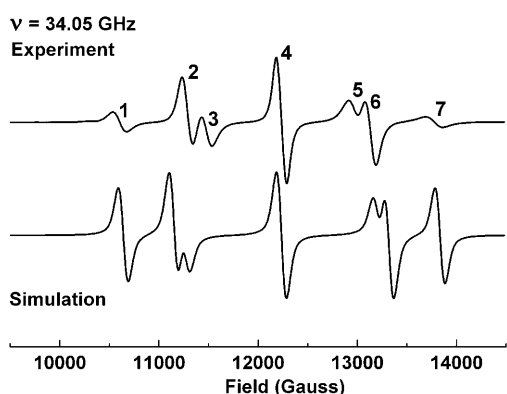


Figure 7. Q-band EPR spectrum of a single crystal of **6** at room temperature. The long axis of the crystal was oriented parallel to the magnetic field. The numbers labeled on the experimental spectrum denote the seven fine structure transitions ($\Delta M_S = \pm 1$) of the Gd^{III} ion.

trum consists of seven lines corresponding to the fine structure of the Gd^{III} ($S=7/2$) ion in an axially symmetric crystal field.^[19] The seven EPR transitions are labeled in Figure 7, using numbers from 1 through 7, and they represent the transitions ΔM_S : $+7/2 \leftrightarrow +5/2$, $+5/2 \leftrightarrow +3/2$, $+3/2 \leftrightarrow +1/2$, $+1/2 \leftrightarrow -1/2$, $-1/2 \leftrightarrow -3/2$, $-3/2 \leftrightarrow -5/2$, $-5/2 \leftrightarrow -7/2$ respectively. Computer simulation of the experimental spectrum using the program Spin^[20] yielded the spin Hamiltonian parameters: $g_{\text{iso}}=1.988$; $D=0.0275 \text{ cm}^{-1}$; $E=0$; $B_4^0=-6.3 \times 10^{-5} \text{ cm}^{-1}$, if $\theta=0^\circ$. The forbidden EPR transitions ($\Delta M_S = \pm 2, \pm 3$) were very weak and poorly resolved and, therefore, are not shown in Figure 7. The compound **5** did not show any EPR lines at room temperature.

Theoretical analysis: DFT calculations were carried out to rationalize some properties of the synthesized compounds. In particular, we have studied the series $[\text{X}^{\text{III}}\text{Pd}^{\text{II}}_{12}(\text{AsR})_8\text{O}_{32}]_n^-$ with $\text{X}=\text{Y}^{\text{III}}$, Lu^{III} , and Gd^{III} . The choice is not arbitrary; the systems with configurations f^0 and f^{14} are much easier to study theoretically than the compounds with an unpaired number of f electrons. Gd^{III} with a $4f^7$ configu-

ration is a special case that can be rather well described at DFT level. For comparison with previous experimental results^[5b] we have also computed **Pd₁₃**, which represents an analogue of the polyanions in **1–13** with the central cation $\text{X}=\text{Pd}^{\text{II}}$ (vide supra). To analyze the effects of the substituents of the external heterogroups we have performed calculations for $\text{R}=\text{H}$ and Ph . For all the computed structures we have found a cubic organization of the eight oxygen atoms around the central cation X . This means that the high coordination of the internal cation has an electronic origin and the potential repulsion between the Ph groups does not cause the particular arrangement observed in **1–13**. In general, the experimental structures are rather well reproduced by calculations, but as we can see from the values in Table 2 the computed distances are always slightly longer than the experimental ones, which in part can be related to the importance of correlation effects in **1–13**.

Table 2. Selected bond lengths [\AA] and atomic charges for several polyoxopalladates $[\text{X}^{\text{III}}\text{Pd}^{\text{II}}_{12}(\text{AsR})_8\text{O}_{32}]_n^-$.

X	R	Unpaired electrons	$2S+1$ ^[a]	$q(\text{X})$ ^[b]	Spin density (X) ^[c]	$q(\text{Pd})$ ^[b]	$d_{\text{X-O}}$ ^[d]
Pd^{II}	H	2	3	+1.24	1.15	+0.88	2.345/2.639
Pd^{II}	Ph	2	3	+1.15	1.15	+0.90	2.396 (2.338)
Y^{III}	H	0	1	+3.11		+0.93	2.396/2.297
Y^{III}	Ph	0	1	+3.07		+0.95	2.384/2.390 (2.346)
(1)							
Gd^{III}	H	7	8	+2.81	6.971	+0.94	2.401/2.402
Lu^{III}	H	0	1	+2.94		+0.95	2.393/2.393
Lu^{III}	Ph	0	1	+2.96		+0.97	2.360/2.362 (2.303)
(13)							

[a] Multiplicity of the computed state; [b] Mulliken atomic charges computed for the central ion and for Pd atoms; [c] Spin densities computed for the central ions; [d] Distances in \AA . Values in parenthesis for X-ray distances.

The atomic charge computed for the central cation is close to +3, if X is a lanthanide or an yttrium atom, confirming the trivalent nature of the cation determined experimentally. As expected the charge transfer is slightly higher for $\text{X}=\text{Y}$ than for the other cases. The HOMO in these structures is a delocalized orbital with contributions of the d_{z^2} , d_{xz} and d_{yz} Pd orbitals, whereas the LUMO is mainly a delocalized $d_{x^2-y^2}$ -like Pd orbital. A 3D representation of these orbitals is given for $\text{X}=\text{Y}$ in the Supporting Information (Figure S1) and for the alpha components of the Gd derivative in Figure 8. The HOMO–LUMO gap (about 1 eV) is significantly lower than that observed in classical POMs (2–3 eV at the same computational level),^[21] which could suggest a smaller stability or higher reactivity of the palladates. The calculations for the open-shell systems have been carried out at unrestricted DFT level in which the alpha and beta orbitals are treated independently. For the Gd derivative, we have only computed the state with multiplicity ($2S+1=8$). The atomic electron spin density for the Gd atom was found to be 6.971 e, a value that indicates that the

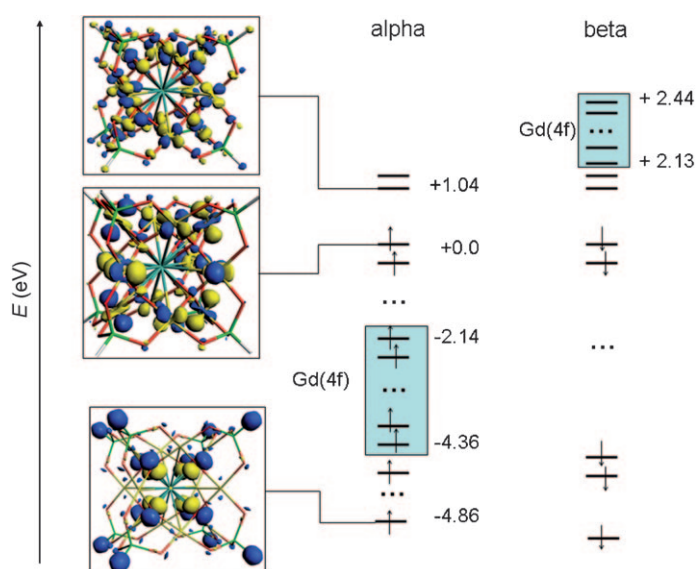


Figure 8. Molecular orbital diagram for the polyanion in **6**. All the energies are referred to the alpha HOMO. Gd (4f) orbitals are spread over several molecular orbitals with energies that range between -4.36 and -2.14 eV for the occupied alpha components and between $+2.13$ and $+2.44$ eV for the beta component. Representations for some selected alpha orbitals are given in Figure S5 in the Supporting Information.

seven unpaired electrons are effectively localized over the lanthanide. As shown in Figure 8, the alpha components of the 4f orbitals are quite profound in relation to the frontier Pd orbitals. The beta counterparts, however, are quite high in energy suggesting that the Gd^{III} ion will not be reduced before the Pd^{II} centers. As shown by electrochemical experiments (vide supra) the lanthanides tend to preserve the 3+ oxidation state. The occupied alpha 4f orbitals are spread in a wide number of molecular orbitals, most of them having a non-bonding nature, as shown in Figure S4 in the Supporting Information. Only one of the orbitals that lies quite low in energy, -4.36 eV with respect to the alpha HOMO, has a bonding nature, but its antibonding counterpart is also occupied (-2.14 eV), therefore we must conclude that the f orbitals do not participate directly in the bond between the lanthanide and the eight neighboring oxygen atoms. Below, we find at -4.86 eV an oxo orbital that is an in phase combination of p orbitals centered at the eight oxygen atoms surrounding the lanthanide (Figure 8). The absence of any relevant contribution from the Gd orbitals is an additional evidence for the ionic nature of the bond between the oxo ligands and the encapsulated ion.

The IR spectrum for the yttrium(III) derivative Na₅[YPd^{II}₁₂(As^VPh)₈O₃₂] \cdot 21 H₂O (**1**) has been computed (see Figure S2 in the Supporting Information). The diagonalization of the second derivatives of the energy shows only positive values confirming that the structure corresponds to a minimum of the potential energy surface. The computed spectrum coincides rather well with the experimental one for **1** (Figure S3 in the Supporting Information). The stretching vibrations of

the AsO₃ group appear between $\tilde{\nu}=711$ and 748 cm⁻¹, whereas the stretching vibrations involving Pd–O(inner) and Pd–O(outer) bonds appear between $\tilde{\nu}=527$ and 531 cm⁻¹ and between $\tilde{\nu}=470$ and 485 cm⁻¹, respectively. In the same region of the spectrum, we can find stretching Y–O vibrations with the two most intense signals at $\tilde{\nu}=342$ and 440 cm⁻¹, respectively.

For comparison with previously characterized heteropolyoxo-13-palladate derivatives, DFT calculations were also carried out on Pd₁₃. When the central position of the palladate is occupied by a Pd^{II} ion the ground state is a triplet, a fact that is supported very well by the observed magnetic properties of this polyanion.^[5b] A triplet ground state has also been found for Pd^{II} in a hexa-coordinated environment.^[22] The Mulliken population analysis (Table 2) and the spin density distribution (Figure 9) clearly indicate that the

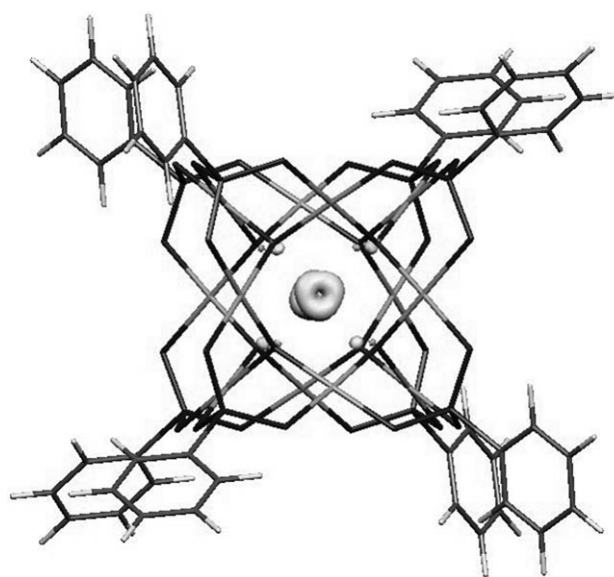


Figure 9. Spin density distribution computed for [Pd^{II}₁₃(AsPh)₈O₃₂]⁶⁻ (**Pd₁₃**).

two unpaired electrons are mainly localized on the central Pd. Mulliken population assigns a spin density (alpha–beta electrons) of 1.15 e localized over the central Pd and a total of 1.78 e if we considered the Pd_{int}–O8 moiety. The HOMO computed for Pd₁₃ is similar to that found for the lanthanide and yttrium derivatives, but the LUMO and LUMO+1 of the beta component indeed are d-orbitals localized on the central or internal Pd. The corresponding occupied alpha components are spread over several molecular orbitals (for more details see Figure S5 in the Supporting Information). The Mulliken population analysis assigns an atomic charge of +1.24e to the internal Pd whereas the corresponding charges for the external metals are a little less positive (+0.88 e). This behavior is easy to rationalize from the higher coordination of the central Pd, which favors the depopulation of the metal. In the Y, Gd, and Lu heteropoly-palladates the electronic population of the outer Pd is slight-

ly higher (0.93–0.97e) likely owed to a more polarized moiety when it encapsulates a trivalent cation.

Conclusion

We have expanded the class of noble metalates by the discovery of a novel family of yttrium(III)- and lanthanide(III)-containing heteropolyoxopalladates, $[X^{III}Pd^{II}_{12}(AsPh)_8O_{32}]^{5-}$ ($X = Y, Pr, Nd, Sm, Eu, Gd, Tb, Dy, Ho, Er, Tm, Yb, \text{ and } Lu$). These polyanions have all been prepared by reaction of $Pd(CH_3COO)_2$, phenylarsonic acid, and the respective yttrium/lanthanide salt in neutral aqueous medium by using conventional open-beaker synthetic techniques. This work extends our earlier studies on heteropoly-13-palladates, in particular $[Pd_{13}(As^VPh)_8O_{32}]^{6-}$ (**Pd₁₃**), which contains an eight-coordinate central Pd^{II} ion. The 13 polyanions reported here are isostructural with **Pd₁₃**, but the central, eight-coordinated Pd^{II} has now been replaced by the larger Y^{III} or Ln^{III} ions ($Ln = \text{lanthanide}$) for which eight-coordination is more common. This is also supported by the yields for **1–13**, which, in general, are significantly higher than for **Na-Pd₁₃**. The $\{Pd_{12}L_8\}$ structure type is a fascinating host which can accommodate a variety of coordination modes of the guests, namely square-planar coordinated Pd^{II} (in $[Pd^{II}_{13}As_8^VO_{34}(OH)_6]^{8-}$), octahedrally coordinated Pd^{II} (in $[Pd_{13}Se_8O_{32}]^{6-}$), cubic coordinated Pd^{II} (in **Na-Pd₁₃**) or Y^{III}/Ln^{III} in **1–13**.^[4a,5] Currently we explore if also 3d metal ions can be incorporated in the $\{Pd_{12}L_8\}$ structure type, and we have already isolated several members. It is evident that the novel POM subclass of noble metalates offers not only new and exciting structures and compositions, but also interesting electronic and potentially functional properties.

Experimental Section

Materials and physical measurements: All reagents were purchased from commercial sources and used without further purification. The IR spectra of **1–13** were recorded on KBr disks by using a Nicolet-Avatar 370 spectrometer between $\tilde{\nu} = 400$ and 4000 cm^{-1} . Thermogravimetric analyses were carried out by using a TA Instruments SDT Q600 thermobalance with a 100 mL min^{-1} flow of nitrogen; the temperature was ramped from 20 to 1200°C at a rate of 5°C min^{-1} . Magnetic measurements on single crystals of **5–6** were performed by using a SQUID magnetometer (Quantum Design MPMS XL). The crystals were oriented with their long axis parallel to the external magnetic field. The dc magnetic susceptibility was measured under a constant magnetic field of 200 Gauss and variable temperature (1.8–300 K) and field-dependent magnetization was measured in the field range 0–7 T, at 1.8 K. The Q-band EPR spectra (34 GHz) of the crystalline samples were measured at room temperature by using a Bruker E-500 spectrometer. Elemental analyses were performed by Mikroanalytisches Labor Pascher, Remagen (Germany) for **13** and by Kanti Labs, Tirupathi (India) for **1–12**.

Na₅[YPd^{II}₁₂(As^VPh)₈O₃₂]-21H₂O (1): $Pd(CH_3COO)_2$ (0.140 g, 0.625 mmol), $PhAsO_3H_2$ (0.125 g, 0.619 mmol), and $Y(NO_3)_3 \cdot 6H_2O$ (0.060 g, 0.156 mmol) were dissolved in 0.5 M sodium acetate solution (5 mL; pH 6.9). While stirring, the solution was heated to 80°C for 90 min. Then it was cooled to room temperature, filtered, and allowed to crystallize at room temperature. Dark red-brown crystals were obtained after several days, filtered off, and air dried. Yield: 0.170 g (43% based

on {Pd}). IR (2% KBr pellet): $\tilde{\nu} = 1629$ (m), 1480 (w), 1439 (m), 1311 (w), 1179 (w), 1161 (w), 1094 (m), 1069 (w), 1024 (w), 1000 (w), 800 (s), 744 (s), 694 (s), 611 (s), 543 (s), 438 cm^{-1} (s); elemental analysis (%) calcd: Na 3.20, Y 2.48, Pd 35.60, As 16.71, C 16.07, H 2.30; found: Na 3.21, Y 2.51, Pd 35.50, As 16.70, C 15.80, H 2.43.

Na₅[PrPd^{II}₁₂(As^VPh)₈O₃₂]-19H₂O (2): The compound was prepared by exactly the same procedure as **1**, but by using $Pr(CH_3COO)_3 \cdot H_2O$ (0.052 g, 0.156 mmol) instead of $Y(NO_3)_3 \cdot 6H_2O$. Dark red-brown crystals were obtained. Yield: 0.035 g (9% based on {Pd}). IR (2% KBr pellet): $\tilde{\nu} = 1631$ (m), 1480 (w), 1440 (m), 1311 (w), 1179 (w), 1162 (w), 1094 (m), 1069 (w), 1025 (w), 1001 (w), 796 (s), 746 (s), 695 (s), 597 (s), 546 (s), 431 cm^{-1} (s); elemental analysis (%) calcd: Na 3.19, Pr 3.91, Pd 35.44, As 16.63, C 16.00, H 2.18; found: Na 3.31, Pr 3.90, Pd 35.30, As 16.40, C 15.80, H 2.41.

Na₅[NdPd^{II}₁₂(As^VPh)₈O₃₂]-24H₂O (3): The compound was prepared by exactly the same procedure as **1**, but by using $Nd(CH_3COO)_3 \cdot H_2O$ (0.053 g, 0.156 mmol). Dark red-brown crystals were obtained. Yield: 0.100 g (26% based on {Pd}). IR (2% KBr pellet): $\tilde{\nu} = 1630$ (m), 1479 (w), 1439 (m), 1310 (w), 1178 (w), 1161 (w), 1093 (m), 1068 (w), 1025 (w), 1001 (w), 797 (s), 744 (s), 695 (s), 598 (s), 545 (s), 434 cm^{-1} (s); elemental analysis (%) calcd: Na 3.11, Nd 3.90, Pd 34.54, As 16.21, C 15.60, H 2.40; found: Na 3.15, Nd 3.65, Pd 34.30, As 16.10, C 15.30, H 2.39.

Na₅[SmPd^{II}₁₂(As^VPh)₈O₃₂]-18H₂O (4): The compound was prepared by exactly the same procedure as **1**, but by using $Sm(NO_3)_3 \cdot 6H_2O$ (0.069 g, 0.156 mmol). Dark red-brown crystals were obtained. Yield: 0.090 g (23% based on {Pd}). IR (2% KBr pellet): $\tilde{\nu} = 1630$ (m), 1480 (w), 1440 (m), 1310 (w), 1179 (w), 1162 (w), 1094 (m), 1068 (w), 1025 (w), 1001 (w), 797 (s), 745 (s), 695 (s), 597 (s), 546 (s), 433 cm^{-1} (s); elemental analysis (%) calcd: Na 3.20, Sm 4.18, Pd 35.52, As 16.67, C 16.04, H 2.13; found: Na 3.24, Sm 4.18, Pd 35.30, As 16.70, C 16.10, H 2.27.

Na₅[EuPd^{II}₁₂(As^VPh)₈O₃₂]-21H₂O (5): The compound was prepared by exactly the same procedure as **1**, but by using $EuCl_3 \cdot 6H_2O$ (0.057 g, 0.156 mmol). Dark red-brown crystals were obtained. Yield: 0.120 g (32% based on {Pd}). IR (2% KBr pellet): $\tilde{\nu} = 1629$ (m), 1479 (w), 1439 (m), 1311 (w), 1180 (w), 1161 (w), 1093 (m), 1069 (w), 1024 (w), 1000 (w), 798 (s), 744 (s), 694 (s), 600 (s), 544 (s), 434 cm^{-1} (s); elemental analysis (%) calcd: Na 3.15, Eu 4.16, Pd 34.98, As 16.42, C 15.79, H 2.26; found: Na 3.15, Eu 4.16, Pd 34.90, As 16.30, C 15.80, H 2.34.

Na₅[GdPd^{II}₁₂(As^VPh)₈O₃₂]-24H₂O (6): The compound was prepared by exactly the same procedure as **1**, but by using $GdCl_3 \cdot 6H_2O$ (0.058 g, 0.156 mmol). Dark red-brown crystals were obtained. Yield: 0.130 g (34% based on {Pd}). IR (2% KBr pellet): $\tilde{\nu} = 1630$ (m), 1480 (w), 1438 (m), 1310 (w), 1179 (w), 1162 (w), 1094 (m), 1068 (w), 1025 (w), 1000 (w), 798 (s), 745 (s), 695 (s), 602 (s), 543 (s), 435 cm^{-1} (s); elemental analysis (%) calcd: Na 3.10, Gd 4.24, Pd 34.42, As 16.16, C 15.54, H 2.39; found: Na 3.14, Gd 4.21, Pd 34.30, As 16.30, C 15.60, H 2.45.

Na₅[TbPd^{II}₁₂(As^VPh)₈O₃₂]-22H₂O (7): The compound was prepared by exactly the same procedure as **1**, but by using $Tb(CH_3COO)_3 \cdot H_2O$ (0.055 g, 0.156 mmol). Dark red-brown crystals were obtained. Yield: 0.125 g (31% based on {Pd}). IR (2% KBr pellet): $\tilde{\nu} = 1629$ (m), 1480 (w), 1438 (m), 1310 (w), 1178 (w), 1162 (w), 1095 (m), 1069 (w), 1024 (w), 1000 (w), 798 (s), 746 (s), 696 (s), 607 (s), 542 (s), 434 cm^{-1} (s); elemental analysis (%) calcd: Na 3.13, Tb 4.32, Pd 34.75, As 16.31, C 15.69, H 2.3; found: Na 3.23, Tb 4.30, Pd 34.70, As 16.10, C 15.70, H 2.41.

Na₅[DyPd^{II}₁₂(As^VPh)₈O₃₂]-19H₂O (8): The compound was prepared by exactly the same procedure as **1**, but by using $DyCl_3 \cdot 6H_2O$ (0.059 g, 0.156 mmol). Dark red-brown crystals were obtained. Yield: 0.095 g (24% based on {Pd}). IR (2% KBr pellet): $\tilde{\nu} = 1628$ (m), 1479 (w), 1438 (m), 1311 (w), 1177 (w), 1161 (w), 1094 (m), 1068 (w), 1025 (w), 1000 (w), 799 (s), 745 (s), 696 (s), 608 (s), 544 (s), 435 cm^{-1} (s); elemental analysis (%) calcd: Na 3.17, Dy 4.48, Pd 35.23, As 16.53, C 15.90, H 2.17; found: Na 3.20, Dy 4.47, Pd 35.20, As 16.30, C 15.80, H 2.24.

Na₅[HoPd^{II}₁₂(As^VPh)₈O₃₂]-16H₂O (9): The compound was prepared by exactly the same procedure as **1**, but by using $HoCl_3 \cdot 6H_2O$ (0.059 g, 0.156 mmol). Dark red-brown crystals were obtained. Yield: 0.130 g (34% based on {Pd}). IR (2% KBr pellet): $\tilde{\nu} = 1627$ (m), 1480 (w), 1439 (m), 1310 (w), 1178 (w), 1162 (w), 1095 (m), 1069 (w), 1025 (w), 1000

(w), 800 (s), 745 (s), 694 (s), 609 (s), 543 (s), 436 cm⁻¹ (s); elemental analysis (%) calcd: Na 3.22, Ho 4.69, Pd 35.74, As 16.77, C 16.13, H 2.03; found: Na 3.18, Ho 4.71, Pd 35.50, As 16.70, C 16.20, H 2.45.

Na₅[ErPd^{II}₁₂(As^VPh)₈O₃₂]-27H₂O (10): The compound was prepared by exactly the same procedure as **1**, but by using Er(CH₃COO)₃·H₂O (0.057 g, 0.156 mmol). Dark red-brown crystals were obtained. Yield: 0.155 g (40% based on {Pd}). IR (2% KBr pellet): $\tilde{\nu}$ = 1626 (m), 1480 (w), 1439 (m), 1310 (w), 1178 (w), 1161 (w), 1094 (m), 1068 (w), 1025 (w), 1000 (w), 799 (s), 744 (s), 695 (s), 610 (s), 544 (s), 435 cm⁻¹ (s); elemental analysis (%) calcd: Na 3.05, Er 4.43, Pd 33.84, As 15.88, C 15.28, H 2.51; found: Na 3.51, Er 4.35, Pd 33.70, As 15.70, C 15.90, H 2.92.

Na₅[TmPd^{II}₁₂(As^VPh)₈O₃₂]-15H₂O (11): The compound was prepared by exactly the same procedure as **1**, but by using TmCl₃·H₂O (0.060 g, 0.156 mmol). Dark red-brown crystals were obtained. Yield: 0.085 g (23% based on {Pd}). IR (2% KBr pellet): $\tilde{\nu}$ = 1623 (m), 1477 (w), 1439 (m), 1309 (w), 1176 (w), 1162 (w), 1095 (m), 1068 (w), 1024 (w), 1000 (w), 800 (s), 744 (s), 695 (s), 613 (s), 542 (s), 436 cm⁻¹ (s); elemental analysis (%) calcd: Na 3.23, Tm 4.75, Pd 35.88, As 16.84, C 16.20, H 1.98; found: Na 2.99, Tm 4.67, Pd 35.90, As 16.90, C 16.40, H 2.43.

Na₅[YbPd^{II}₁₂(As^VPh)₈O₃₂]-18H₂O (12): The compound was prepared by exactly the same procedure as **1**, but by using Yb(NO₃)₃·5H₂O (0.070 g, 0.156 mmol). Dark red-brown crystals were obtained. Yield: 0.160 g (42% based on {Pd}). IR (2% KBr pellet): $\tilde{\nu}$ = 1628 (m), 1480 (w), 1440 (m), 1311 (w), 1178 (w), 1161 (w), 1094 (m), 1066 (w), 1025 (w), 999 (w), 799 (s), 745 (s), 695 (s), 612 (s), 543 (s), 435 cm⁻¹ (s); elemental analysis (%) calcd: Na 3.18, Yb 4.78, Pd 35.3, As 16.57, C 15.94, H 2.12; found: Na 2.97, Yb 4.62, Pd 35.30, As 16.20, C 16.10, H 2.47.

Na₅[LuPd^{II}₁₂(As^VPh)₈O₃₂]-16H₂O (13): The compound was prepared by exactly the same procedure as **1**, but by using LuCl₃·6H₂O (0.061 g, 0.156 mmol). Dark red-brown crystals were obtained. Yield: 0.120 g (32% based on {Pd}). IR (2% KBr pellet): $\tilde{\nu}$ = 1624 (m), 1479 (w), 1439 (m), 1310 (w), 1178 (w), 1161 (w), 1095 (m), 1068 (w), 1025 (w), 1001 (w), 801 (s), 743 (s), 694 (s), 614 (s), 541 (s), 438 cm⁻¹ (s); elemental analysis (%) calcd: Na 3.21, Lu 4.88, Pd 35.64, As 16.73, C 16.09, H 2.03; found: Na 3.10, Lu 4.30, Pd 35.50, As 16.20, C 16.10, H 2.20.

X-ray crystallography: Data for the structures of **1–13** were collected at 173 K by using a Bruker Kappa X8 APEX CCD single-crystal diffractometer equipped with a sealed Mo tube and graphite monochromator ($l = 0.71073$ Å). Crystals were mounted in Hampton cryoloops with light oil to prevent water loss. The SHELX software package (Bruker) was used to solve and refine the structures.^[23] Absorption corrections were applied empirically using the SADABS program.^[24] The structures were solved by direct methods and refined by the full-matrix least-squares method minimization of $(\sum w(F_o - F_c)^2)$ with anisotropic thermal parameters for all POM skeleton non-hydrogen atoms. The hydrogen atoms of the phenyl rings in **1–13** were introduced in geometrically calculated positions. The H atoms of the crystal waters were not localized in any of the compounds. The Na counter cations in all structures were highly disordered and could not be located by XRD, which is a common problem in POM crystallography. However we clearly identified the presence of five Na⁺ ions in **1–13** by elemental analyses. Additional crystallographic data are summarized in Tables S1–S3 (see the Supporting Information).

CCDC-751303 (**1**), CCDC-751304 (**2**), CCDC-751305 (**3**), CCDC-751306 (**4**), CCDC-751307 (**5**), CCDC-751308 (**6**), CCDC-751309 (**7**), CCDC-751310 (**8**), CCDC-751311 (**9**), CCDC-751312 (**10**), CCDC-751313 (**11**), CCDC-751314 (**12**), and CCDC-751315 (**13**) contain the supplementary crystallographic data for this paper. These data can be obtained free of charge from The Cambridge Crystallographic Data Centre via www.ccdc.cam.ac.uk/data_request/cif

Electrochemistry: For the electrochemical experiments, the source, mounting and polishing of the glassy carbon (GC, Le Carbone Lorraine, France) electrodes has been described previously.^[25] The electrochemical set-up was an EG & G 273 A driven by a PC with the M270 software. Potentials were measured against a saturated calomel reference electrode (SCE). The counter electrode was a platinum gauze of large surface area. Pure water from a RiOs 8 unit followed by a Millipore-Q Academic purification set was used throughout. The solutions were deaerated thoroughly for at least 30 min with pure argon and kept under a positive pres-

sure of this gas during the experiments. The supporting electrolyte was a pH 5.9 buffer solution (1 M CH₃COOLi + CH₃COOH).

Computational details: Calculations were carried out using DFT methodology with the ADF 2007 program.^[26] The exchange-correlation functionals of Becke and Perdew were used.^[27–28] Relativistic corrections were included by means of the ZORA formalism. Triple- ζ + polarization basis sets were employed to describe the valence electrons of the C, O, As, H, Pd, Y, Gd, and Lu atoms. Frozen cores consisting of: i) the 1s shell for C, O; ii) the 1s to 2p shells for As; iii) the 1s to 3d shells for Y; and iv) the 1s to 4d for Gd and Lu were described by means of single Slater functions. All the structures have been optimized without symmetry restrictions. The calculations for open-shell structures were carried out at the unrestricted level.

Acknowledgements

U.K. thanks the German Science Foundation (DFG-KO-2288/9-1), the Fonds der Chemischen Industrie and Jacobs University for research support. We thank Dr. M. H. Dickman for help with XRD. The University Paris Sud 11 and the CNRS (UMR 8000) are thanked for research support. J.M.P. thanks the MICINN of Spain (CTQ2008-06549-C02-01) and the Generalitat de Catalunya (2009SGR00462 and XRQTC) for financial support. N.S.D. thanks NSF-DMR 0506946 for work at FSU.

- [1] a) M. T. Pope, *Heteropoly and Isopoly Oxometalates*, Springer, Berlin, **1983**; b) V. W. Day, W. G. Klemperer, *Science* **1985**, *228*, 533–541; c) M. T. Pope, A. Müller, *Angew. Chem.* **1991**, *103*, 56–70; *Angew. Chem. Int. Ed. Engl.* **1991**, *30*, 34–48; d) S. S. Talismanov, I. L. Eremenko, *Russ. Chem. Rev.* **2003**, *72*, 555–569; e) *Cronin in Comprehensive Coordination Chemistry II, Vol. 7* (Eds.: J. A. McCleverty, T. J. Meyer), Elsevier, Amsterdam, **2004**, pp. 1–57; f) B. Hasenknopf, K. Micoine, E. Lacote, S. Thorimbert, M. Malacria, R. Thouvenot, *Eur. J. Inorg. Chem.* **2008**, 5001–5013; g) *Eur. J. Inorg. Chem.* **2009**, *34*, edited by U. Kortz (issue dedicated to polyoxometalates).
- [2] a) *Polyoxometalates: From Platonic Solids to Antiretroviral Activity* (Eds.: M. T. Pope, A. Müller), Kluwer, Dordrecht, **1994**; b) T. Okuhara, N. Mizuno, M. Misono, *Adv. Catal.* **1996**, *41*, 113–252; c) *Chem. Rev.* **1998**, *98*, edited by C. L. Hill (special issue on polyoxometalates); d) A. Müller, S. Roy, *Coord. Chem. Rev.* **2003**, *245*, 153–166; e) E. Coronado, P. Day, *Chem. Rev.* **2004**, *104*, 5419–5448; f) C. L. Hill, *J. Mol. Catal. A* **2007**, *262*, 2–6; g) U. Kortz, A. Müller, J. van Slageren, J. Schnack, N. S. Dalal, M. Dressel, *Coord. Chem. Rev.* **2009**, *253*, 2315–2327.
- [3] a) M. Pley, M. S. Wickleder, *Angew. Chem.* **2004**, *116*, 4262–4264; *Angew. Chem. Int. Ed. Engl.* **2004**, *43*, 4168–4170; b) M. Pley, M. S. Wickleder, *Z. Naturforsch. B* **2006**, *61*, 912–915.
- [4] a) E. V. Chubarova, M. H. Dickman, B. Keita, L. Nadjo, F. Miserque, M. Mifsud, I. W. C. E. Arends, U. Kortz, *Angew. Chem.* **2008**, *120*, 9685–9689; *Angew. Chem. Int. Ed.* **2008**, *47*, 9542–9546; b) J. C. Goloboy, W. G. Klemperer, *Angew. Chem.* **2009**, *121*, 3614–3616; *Angew. Chem. Int. Ed.* **2009**, *48*, 3562–3564; c) N. V. Izarova, N. Vankova, T. Heine, R. N. Biboum, B. Keita, L. Nadjo, U. Kortz, *Angew. Chem.* **2010**, *122*, 1930–1933; *Angew. Chem. Int. Ed.* **2010**, *49*, 1886–1889.
- [5] a) N. V. Izarova, R. N. Biboum, B. Keita, M. Mifsud, I. W. C. E. Arends, G. B. Jameson, U. Kortz, *Dalton Trans.* **2009**, 9385–9387; b) N. V. Izarova, M. H. Dickman, R. N. Biboum, B. Keita, L. Nadjo, V. Ramachandran, N. S. Dalal, U. Kortz, *Inorg. Chem.* **2009**, *48*, 7504–7506; c) M. Delferro, C. Graiff, L. Elviri, G. Predieri, *Dalton Trans.* **2010**, *39*, 4479–4481.
- [6] a) I. Creaser, M. C. Heckel, R. J. Neitz, M. T. Pope, *Inorg. Chem.* **1993**, *32*, 1573–1578; b) C. Zhang, R. C. Howell, K. B. Scotland, F. G. Perez, L. Todaro, L. C. Francesconi, *Inorg. Chem.* **2004**, *43*, 7691–7701; c) Q.-M. Wang, B. Yan, *Inorg. Chem. Commun.* **2004**, *7*,

- 1124–1127; d) C. Boglio, G. Lemiere, B. Hasenknopf, S. Thorimbert, E. Lacote, M. Malacria, *Angew. Chem.* **2006**, *118*, 3402–3405; *Angew. Chem. Int. Ed.* **2006**, *45*, 3324–3327; e) C. Boglio, G. Lenoble, C. Duhayon, B. Hasenknopf, R. Thouvenot, C. Zhang, R. C. Howell, B. P. Burton-Pye, L. C. Francesconi, E. Lacôte, S. Thorimbert, M. Malacria, C. Afonso, J.-C. Tabet, *Inorg. Chem.* **2006**, *45*, 1389–1398; f) W. Huang, L. C. Francesconi, T. Polenova, *Inorg. Chem.* **2007**, *46*, 7861–7869; g) M. A. AlDamen, S. Cardona-Serra, J. M. Clemente-Juan, E. Coronado, A. Gaita-Ariño, C. Martí-Gastaldo, F. Luis, O. Montero, *Inorg. Chem.* **2009**, *48*, 3467–3479.
- [7] a) K. Wassermann, M. H. Dickman, M. T. Pope, *Angew. Chem.* **1997**, *109*, 1513–1516; *Angew. Chem. Int. Ed. Engl.* **1997**, *36*, 1445–1448; b) R. C. Howell, F. G. Perez, S. Jain, W. D. W. J. Horrocks, A. L. Rheingold, L. C. Francesconi, *Angew. Chem.* **2001**, *113*, 4155–4158; *Angew. Chem. Int. Ed.* **2001**, *40*, 4031–4034; c) G. L. Xue, J. Vaissermann, P. Gouzerh, *J. Cluster Sci.* **2002**, *13*, 409–421; d) N. V. Izarova, M. N. Sokolov, D. G. Samsonenko, A. Rothenberger, D. Yu. Naumov, D. Fenske, V. P. Fedin, *Eur. J. Inorg. Chem.* **2005**, 4985–4996; e) N. V. Izarova, M. N. Sokolov, D. G. Samsonenko, A. Rothenberger, D. Fenske, V. P. Fedin, *Russ. Chem. Bull.* **2008**, *57*, 78–82; f) A. H. Ismail, M. H. Dickman, U. Kortz, *Inorg. Chem.* **2009**, *48*, 1559–1565; g) F. Hussain, B. Spingler, F. Conrad, M. Speldrich, P. Kögerler, C. Boskovic, G. R. Patzke, *Dalton Trans.* **2009**, *23*, 4423–4425; h) F. Hussain, R. W. Gable, M. Speldrich, P. Kögerler, C. Boskovic, *Chem. Commun.* **2009**, 328–330; i) F. Hussain, F. Conrad, G. R. Patzke, *Angew. Chem.* **2009**, *121*, 9252–9255; *Angew. Chem. Int. Ed.* **2009**, *48*, 9088–9091.
- [8] a) M. Nishio, *CrystEngComm* **2004**, *6*, 130–158; b) M. Nishio, M. Hirota, Y. Umezawa, *The CH/π Interaction: Evidence, Nature and Consequences*, Wiley-VCH, Weinheim, **1998**.
- [9] L. Helsen, E. Van den Bulck, M. K. Van Bael, G. Vanhoyland, J. Mullens, *Thermochim. Acta* **2004**, *414*, 145–153.
- [10] N. B. Mikheev, S. A. Kulyukhin, I. V. Melikhov, *Radiochemistry* **2007**, *49*, 393–406.
- [11] I. V. Martynov, *Russian J. Inorg. Chem.* **2008**, *53*, 579–582.
- [12] R. C. Weast, *Handbook of Chemistry and Physics*, 66th ed., CRC Press, Boca Raton, **1986**, pp. 153–155.
- [13] a) L.-H. Bi, M. Reike, U. Kortz, B. Keita, L. Nadjo, R. J. Clark, *Inorg. Chem.* **2004**, *43*, 3915–3920; b) L.-H. Bi, U. Kortz, B. Keita, L. Nadjo, L. Daniels, *Eur. J. Inorg. Chem.* **2005**, 3034–3041; c) L.-H. Bi, U. Kortz, B. Keita, L. Nadjo, H. Borrmann, *Inorg. Chem.* **2004**, *43*, 8367–8372.
- [14] Representative papers on Pd⁰ deposition from Pd^{II} solutions and its electrochemical behaviors include: a) K.-H. Lubert, M. Guttman, L. J. Beyer, *Electroanal. Chem.* **1999**, *462*, 174–180; b) K.-H. Lubert, M. Guttman, L. Beyer, K. Kalcher, *Electrochem. Commun.* **2001**, *3*, 102–106; c) X.-G. Zhang, T. Arikawa, Y. Murakami, K. Yahikozawa, Y. Takasu, *Electrochim. Acta* **1995**, *40*, 1889–1897; d) M. J. Ball, C. A. Lucas, N. M. Markovic, V. Stamenkovic, P. N. Ross, *Surfactant Sci. Ser.* **2002**, *518*, 201–209; e) X. Q. Tong, M. Aindow, J. P. G. Farr, *J. Electroanal. Chem.* **1995**, *395*, 117–126; f) N. Tateishi, K. Yahikozawa, K. Nashimura, M. Suzuki, Y. Iwanaga, M. Watanabe, E. Enami, Y. Matsuda, Y. Takasu, *Electrochim. Acta* **1991**, *36*, 1235–1240; g) X.-G. Zhang, Y. Murakami, K. Yahikozawa, Y. Takasu, *Electrochim. Acta* **1997**, *42*, 223–227; h) N. M. Markovic, C. A. Lucas, V. Climent, V. Stamenkovic, P. N. Ross, *Surfactant Sci. Ser.* **2000**, *465*, 103–114; i) L.-J. Wan, T. Suzuki, K. Sashikata, J. Okada, J. Inukai, K. Itaya, *J. Electroanal. Chem.* **2000**, *484*, 189–193; j) A. M. El-Aziz, L. A. Kibler, D. M. Kolb, *Electrochem. Commun.* **2002**, *4*, 535–539; k) M. Arenz, V. Stamenkovic, T. J. Schmidt, K. Wandelt, P. N. Ross, N. M. Markovic, *Surfactant Sci. Ser.* **2003**, *523*, 199–209.
- [15] C.-C. Hu, T.-C. Wen, *Electrochim. Acta* **1996**, *41*, 1505–1514.
- [16] a) U. Kortz, S. Nellutla, A. C. Stowe, N. S. Dalal, J. van Tol, B. S. Bassil, *Inorg. Chem.* **2004**, *43*, 144–154; b) U. Kortz, S. Nellutla, A. C. Stowe, N. S. Dalal, U. Rauwald, D. Welbeck, D. Ravot, *Inorg. Chem.* **2004**, *43*, 2308–2317.
- [17] R. L. Carlin, *Magetochimistry*, Springer, Berlin, **1986**.
- [18] a) E. del Barco, J. M. Hernandez, J. Tejada, N. Biskup, R. Achey, I. Rutel, N. Dalal, J. Brooks, *Phys. Rev. B* **2000**, *62*, 3018–3021; b) E. del Barco, A. D. Kent, S. Hill, J. M. North, N. S. Dalal, E. M. Rumberger, D. N. Hendrickson, N. Chakov, G. Christou, *J. Low Temp. Phys.* **2005**, *140*, 119–174; c) N. E. Chakov, S.-C. Lee, A. G. Harter, P. L. Kuhns, A. P. Reyes, S. O. Hill, N. S. Dalal, W. Wernsdorfer, K. A. Abboud, G. Christou, *J. Am. Chem. Soc.* **2006**, *128*, 6975–6989.
- [19] A. Abragam, B. Bleaney, *Electron Paramagnetic Resonance of Transition Ions*; Oxford University Press, Oxford, **1970**.
- [20] A. Ozarowski, *Spin*, National High Magnetic Field Laboratory, Tallahassee.
- [21] a) J. M. Poblet, X. López, C. Bo, *Chem. Soc. Rev.* **2003**, *32*, 297–308; b) J. A. Fernández, X. López, C. Bo, C. de Graaf, E. J. Baerends, J. M. Poblet, *J. Am. Chem. Soc.* **2007**, *129*, 12244–12253; c) L. Yan, X. López, J. J. Carbó, R. T. Sniatynsky, D. D. Duncan, J. M. Poblet, *J. Am. Chem. Soc.* **2008**, *130*, 8223–8233.
- [22] F. Pointillart, C. Train, F. Villain, C. C. dit Moulin, P. Gredin, L.-M. Camoreau, M. Gruselle, G. Aullon, S. Alvarez, M. J. Verdager, *J. Am. Chem. Soc.* **2007**, *129*, 1327–1334.
- [23] G. M. Sheldrick, *Acta Crystallogr. Sect. A* **2007**, *64*, 112–122.
- [24] SADABS, Program for empirical X-ray absorption correction, G. M. Sheldrick, Bruker-Nonius, **1990**.
- [25] B. Keita, L. Nadjo, *J. Electroanal. Chem.* **1988**, *243*, 87–103.
- [26] a) A. Klamt, G. K. Schüürmann, *J. Chem. Soc. Perkin Trans. 2* **1993**, 799–805; b) J. Andzelm, C. Kölmel, A. Klamt, *J. Chem. Phys.* **1995**, *103*, 9312–9320; c) A. J. Klamt, *Chem. Phys.* **1995**, *190–201*, 2224–2235. Method implemented in the ADF package by: d) C. C. Pye, T. Ziegler, *Theor. Chem. Acc.* **1999**, *101*, 396–408.
- [27] a) A. D. Becke, *J. Chem. Phys.* **1986**, *84*, 4524–4529; b) A. D. Becke, *Phys. Rev.* **1988**, *A38*, 3098–3100.
- [28] a) J. P. Perdew, *Phys. Rev. B* **1986**, *33*, 8822–8824; b) J. P. Perdew, *Phys. Rev. B* **1986**, *34*, 7406–7406.

Received: March 11, 2010

Published online: June 29, 2010